Draft version May 8, 2020
Preprint typeset using LaTeX style emulateapj v. 08/13/06

SPECKLE INTERFEROMETRY AT SOAR IN 2019

Andrei Tokovinin
Cerro Tololo Inter-American Observatory,* Casilla 603, La Serena, Chile

Brian D. Mason
U.S. Naval Observatory, 3450 Massachusetts Ave., Washington, DC, USA

Rene A. Mendez
Universidad de Chile, Casilla 36-D, Santiago, Chile

Edgardo Costa
Universidad de Chile, Casilla 36-D, Santiago, Chile

Elliott P. Horch†
Department of Physics, Southern Connecticut State University, 501 Crescent Street, New Haven, CT 06515, USA
Draft version May 8, 2020

ABSTRACT

The results of speckle interferometric observations at the 4.1 m Southern Astrophysical Research Telescope (SOAR) in 2019 are given, totaling 2555 measurements of 1972 resolved pairs with separations from 15 mas (median 0.″21) and magnitude difference up to 6 mag, and non-resolutions of 684 targets. We resolved for the first time 90 new pairs or subsystems in known binaries. This work continues our long-term speckle program. Its main goal is to monitor orbital motion of close binaries, including members of high-order hierarchies and *Hipparcos* pairs in the solar neighborhood. We give a list of 127 orbits computed using our latest measurements. Their quality varies from excellent (25 orbits of grades 1 and 2) to provisional (47 orbits of grades 4 and 5).

Subject headings: binaries:visual

1. INTRODUCTION

We report here a large set of double-star measurements made at the 4.1 m Southern Astrophysical Research Telescope (SOAR) with the speckle camera, HRCam. This paper continues the series published by Tokovinin, Mason, & Hartkopf (2010a, hereafter TMH10), Tokovinin et al. (2010b), Hartkopf et al. (2012), Tokovinin (2012), Tokovinin et al. (2014), Tokovinin et al. (2015), Tokovinin et al. (2016a), Tokovinin et al. (2018), and Tokovinin et al. (2019). The aims are outlined in these papers and briefly recalled below. The data were taken during 2019. They are presented in the same format as in Tokovinin et al. (2019).

Section 2 reviews all speckle programs executed at SOAR in 2019. The results are presented in Section 3 in the form of electronic tables archived by the journal. We also discuss new resolutions and provide a large list of new orbital elements. A short summary in Section 4 closes the paper.

2. OBSERVATIONS

2.1. *Observing programs*

As in previous years, HRCam (see Sect. 2.2) was used during 2019 to execute several observing programs, some with common (overlapping) targets. Table 1 gives an overview of these programs and indicates which observations are published in the present paper. Here is a brief description of these programs.

Orbits of resolved binaries are of fundamental importance in various areas of astronomy, e.g. for direct measurement of stellar masses, binary statistics, astrometry, and objects of special interest such as binaries hosting exo-planets. Observations of tight pairs with fast motion, mostly nearby dwarfs, are prioritized at SOAR. However, classical visual binaries are also observed at low cadence to improve their orbits. The Sixth Catalog of Visual Binary Star Orbits, VB6 (Hartkopf, Mason & Worley 2001), contains a substantial fraction of poorly determined, low-grade orbits based on inaccurate and/or sparse visual micrometric measures. This situation is slowly improving. Our work has added many orbits to VB6, more are given here in Section 3.3.

Hierarchical systems of stars challenge the theories of binary-star formation. Better observational data on their statistics and architecture (orbits, relative inclinations) are needed (Tokovinin 2018b). Many hierarchies have been discovered at SOAR using HRCam, and we are following their orbital motion. This paper adds several newly discovered hierarchies and several orbits of subsystems.

*National Science Foundation's National Optical-Infrared Astronomy Research Laboratory
Electronic address: atokovinin@ctio.noao.edu
Electronic address: brian.d.mason@navy.mil
Electronic address: rmendez@u.uchile.cl
†Adjunct Astronomer, Lowell Observatory
Electronic address: horche2@southernct.edu

TABLE 1
Observing programs executed with HRCam in 2019

Program	PI	N	Publ.[a]
Orbits	Mason, Tokovinin	996	Yes
Hierarchical systems	Tokovinin	188	Yes
Hipparcos binaries	Mendez, Horch	737	Yes
Neglected binaries	R. Gould, Tokovinin	363	Yes
Binaries in Upper Scorpius	Tokovinin, Briceño,	485	Pub
Nearby K,M dwarfs	E. Vrijmoet	453	No
TESS follow-up	C. Ziegler	785	Pub
Young moving groups	A. Mann	645	No
Stars with RV trends	B. Pantoja	48	No

[a]This columns indicates whether the results are published here (Yes), previously (Pub), or deferred to future papers (No).

Hipparcos binaries (Perryman et al. 1997) within 200 pc are monitored with the aim of determining orbits and masses for stars in a wide range of effective temperatures and metallicities, as outlined by Horch et al. (2015, 2017, 2019). The southern part of this sample is addressed at SOAR (Mendez et al. 2017). This program overlaps with the general work on orbits.

Accurate parallaxes of visual binaries combined with good-quality orbits will allow accurate measurements of stellar masses. However, the parallactic and orbital motions are coupled. The second *Gaia* data release, DR2 (Gaia collaboration 2018), uses only a linear 5-parameter astrometric model and contains examples of biased parallaxes and proper motions of tight visual binaries. Including acceleration and higher-order terms in the astrometric solution will improve the situation, but the ultimate astrometric precision will be reached only when the orbit is explicitly included in the astrometric model. Considering the limited duration of the *Gaia* mission, ground-based coverage is and will remain essential for accurate measurements of stellar masses.

Neglected binaries with small separations from the Washington Double Star Catalog, WDS (Mason et al. 2001) are observed with a low priority, as a "filler". Lists of pairs in need of fresh data are provided by R. Gould. A fraction of these stars are interesting because they are presently very tight, near the periastron of their orbits. Some of these pairs contain additional, previously unknown, components.

Members of the Upper Scorpius association were surveyed in a systematic way by Tokovinin & Briceño (2020) to find multiplicity fraction and the distribution of periods and mass ratios, taking advantage of the high productivity of HRCam. The work started in 2018. A total of 614 targets were observed during 2018 and 2019 using approximately two nights of telescope time. Several interesting results are reported in the above paper. Moreover, new close pre-main sequence pairs with fast orbital motion are excellent candidates for measuring masses and testing evolutionary models of young stars.

Nearby K and M dwarfs were observed for E. Vrijmoet. His program aims at determination of a large number of orbits to throw new light on the statistics of orbital elements. As these stars are nearby, some have very short orbital periods and displayed a substantial orbital motion during 2019.

TESS follow-up was one of the major observing programs during 2019. Its first results are published by Ziegler et al. (2020), but observations continued since the submission of this paper, and the number of surveyed TESS objects of interests has almost doubled.

If observations of a given star were requested by several programs, they are published here even if the other program still continues. We also publish measurements of previously known pairs resolved during surveys, for example in the TESS follow-up.

2.2. *Instrument and observing procedure*

The observations reported here were obtained with the *high-resolution camera* (HRCam) – a fast imager designed to work at the 4.1 m SOAR telescope (Tokovinin 2018a). The camera was mounted on the SOAR Adaptive Module (SAM, Tokovinin et al. 2016b). The laser guide star of SAM was not used, the deformable mirror of SAM was passively flattened, and the images are seeing-limited. However, the atmospheric dispersion corrector (ADC) inside SAM was critical for getting good-quality data. In most observing runs, the median image size was $\sim 0\farcs6$. The transmission curves of HRCam filters are given in the instrument manual.[1] We used mostly the near-infrared I filter (824/170 nm) and the Strömgren y filter (543/22 nm); two measures were made in the R filter (596/121 nm) and two in the Hα filter (657.3/5 nm).

For each observing run, a selection of suitable targets from all programs was made. It contains accurate coordinates and proper motions (PMs) to allow for precise pointing of the telescope. The slews are commanded from the custom observing tool that helps to maximize the observing efficiency. When the slew angle is small, the next object is acquired almost immediately. Most observations were taken in the narrow $3''$ field with the 200×200 region of interest (ROI), without binning, in the I filter; the y filter was used mostly for brighter and/or closer pairs. The pixel scale is $0\farcs01575$ and the exposure time is normally 24 ms (it is limited by the camera readout speed). Pairs wider than $\sim 1\farcs4$ are observed in a 400×400 ROI, and the widest pairs are sometimes recorded with the full field of 1024 pixels ($16''$) and 2×2 binning. However, the speckle contrast drops very strongly at separations above $3''$, substantially reducing the quality of measures of wide pairs. Binning is used mostly for the fainter targets; it does not result in the loss of resolution in the I band, which ranges from 40 to 45 mas, depending on the magnitude and conditions. Bright stars can be resolved and measured below the formal diffraction limit by fitting a model to the power spectrum and using observations of point sources as reference. The resolution and contrast limits of HRCam are further discussed in TMH10 and in previous papers of this series. For each target, two data cubes of 400 frames are normally recorded and processed independently. This ensures reliability of results despite occasional problems like cosmic ray spikes or telescope vibration.

The first observations reported here were obtained in 2019 January, and the last in 2019 December, in 9 observing runs. HRCam was used during scheduled observing time, but also in parts of engineering nights available from other work. The total number of observations in 2019 (including reference stars) is 5964; the vast majority (5242) are made in the I filter, while for bright and

[1] http://www.ctio.noao.edu/soar/sites/default/files/SAM/-archive/hrcaminst.pdf

close pairs we used the y filter (714 observations). The full set of the 2019 data counts 3199 measurements of 2774 resolved pairs, mostly (but not entirely) published here. Almost all targets are brighter than $I = 12$ mag, although several fainter pairs were measured under very good seeing.

2.3. *Data processing and calibration*

The data processing is described in TMH10 and Tokovinin (2018a) and briefly recalled here. We use the standard speckle interferometry technique based on the calculation of the power spectrum and the speckle autocorrelation function (ACF) derived from it. Companions are detected as secondary peaks in the ACF and/or as fringes in the power spectrum. Parameters of the binary and triple stars (separation ρ, position angle θ, and magnitude difference Δm) are determined by modeling the observed power spectrum. Additionally, the true quadrant is found from the shift-and-add images, whenever possible.

The pixel scale and angular offset are determined by observations of several relatively wide calibration binaries. Their motion is modeled based on previous observations at SOAR, with individual scale and orientation corrections for each observing run. The models are adjusted iteratively (the latest adjustment in 2019 November). Measurements of wide calibrators by *Gaia* show very small systematic errors (Tokovinin et al. 2019). Typical rms deviations of observations of calibrators from their models are 0.°2 in angle and 1 to 3 mas in separation. The position accuracy strongly depends on the target characteristics (larger errors at large Δm and for faint pairs), as well as on the seeing and telescope vibration.

Figure 1 plots the magnitude difference vs. separation for pairs resolved in the I filter (a similar plot was given in Tokovinin et al. 2019). The upper envelope gives a clear idea of the typical contrast limit vs. separation. Several points above the envelope correspond to very difficult tight pairs with a large ΔI; these measures, made at or beyond the limit of the technique, have large errors. Note points to the left of the formal diffraction limit (vertical dotted line, 41 mas).

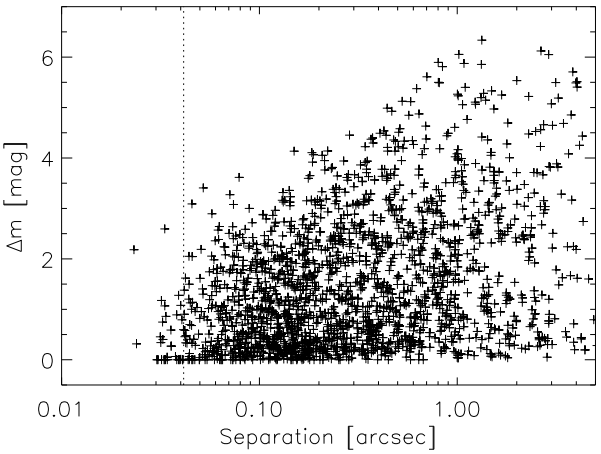

FIG. 1.— Magnitude difference in the I band vs. separation for pairs resolved in this filter. The vertical dotted line marks the formal diffraction limit of 41 mas.

TABLE 2
MEASUREMENTS OF DOUBLE STARS AT SOAR

Col.	Label	Format	Description, units
1	WDS	A10	WDS code (J2000)
2	Discov.	A16	Discoverer code
3	Other	A12	Alternative name
4	RA	F8.4	R.A. J2000 (deg)
5	Dec	F8.4	Declination J2000 (deg)
6	Epoch	F9.4	Julian year (yr)
7	Filt.	A2	Filter
8	N	I2	Number of averaged cubes
9	θ	F8.1	Position angle (deg)
10	$\rho\sigma_\theta$	F5.1	Tangential error (mas)
11	ρ	F8.4	Separation (arcsec)
12	σ_ρ	F5.1	Radial error (mas)
13	Δm	F7.1	Magnitude difference (mag)
14	Flag	A1	Flag of magnitude difference[a]
15	$(O-C)_\theta$	F8.1	Residual in angle (deg)
16	$(O-C)_\rho$	F8.3	Residual in separation (arcsec)
17	Ref.	A8	Orbit reference[b]

[a]Flags: q – the quadrant is determined; * – Δm and quadrant from average image; : – noisy data.
[b]References to VB6 are provided at http://ad.usno.navy/mil/wds/orb6/wdsref.txt

3. RESULTS

3.1. *Data tables*

The results (measures of resolved pairs and non-resolutions) are presented in the same format as in Tokovinin et al. (2019). The long tables are published electronically; here we describe their content.

Table 2 lists 2555 measures of 1972 resolved pairs and subsystems, including the new discoveries. The pairs are identified by their WDS codes and discoverer designations adopted in the WDS catalog (Mason et al. 2001), as well as by alternative names in column (3), mostly from the *Hipparcos* catalog. Equatorial coordinates for the epoch J2000 in degrees are given in columns (4) and (5) to facilitate matching with other catalogs and databases. In the case of resolved multiple systems, the position measurements and their errors (columns 9–12) and magnitude differences (column 13) refer to the individual pairings between components, not to their photo-centers. As in the previous papers of this series, we list the internal errors derived from the power spectrum model and from the difference between the measures obtained from two data cubes. The median error is 0.4 mas, and 90% of errors are less than 1.8 mas. The real errors are usually larger, especially for difficult pairs with substantial Δm and/or with small separations. Residuals from orbits (Section 3.3) and from the models of calibrators, typically between 1 and 5 mas rms, characterize the external errors of the HRcam astrometry.

The flags in column (14) indicate cases when the true quadrant is determined (otherwise the position angle is measured modulo 180°), when the photometry of wide pairs is derived from the long-exposure images (this reduces the bias caused by speckle anisoplanatism) and when the data are noisy or the resolutions are tentative (see TMH10). For binary stars with known orbits, the residuals to the latest orbit and its reference are provided in columns (15)–(17). This work is referenced as SOAR2019.

Non-resolutions are reported in Table 3. Its first columns (1) to (8) have the same meaning and format as in Table 2. Column (9) gives the minimum resolvable

TABLE 3
Unresolved stars

Col.	Label	Format	Description, units
1	WDS	A10	WDS code (J2000)
2	Discov.	A16	Discoverer code
3	Other	A12	Alternative name
4	RA	F8.4	R.A. J2000 (deg)
5	Dec	F8.4	Declination J2000 (deg)
6	Epoch	F9.4	Julian year (yr)
7	Filt.	A2	Filter
8	N	I2	Number of averaged cubes
9	$\rho_{\rm min}$	F7.3	Angular resolution (arcsec)
10	$\Delta m(0.15)$	F7.2	Max. Δm at $0\farcs15$ (mag)
11	$\Delta m(1)$	F7.2	Max. Δm at $1''$(mag)
12	Flag	A1	: marks noisy data

separation when pairs with $\Delta m < 1$ mag are detectable. It is computed from the maximum spatial frequency of the useful signal in the power spectrum and is normally close to the formal diffraction limit λ/D. The following columns (10) and (11) provide the indicative dynamic range, i.e. the maximum magnitude difference at separations of $0\farcs15$ and $1''$, respectively. The last column (12) marks noisy data by the flag ":".

Table 2 contains 90 pairs resolved for the first time; some of those were confirmed in subsequent observing runs. Additional first resolutions belonging to the projects led by other PIs will be reported elsewhere (these pairs are not published here), while new pairs discovered in Upper Scorpius are published by Tokovinin & Briceño (2020). In the following sub-section we discuss the new pairs.

3.2. *New pairs*

TABLE 4
New double stars

WDS	Name	ρ (arcsec)	Δm (mag)	Program[a]
00160−4816	HIP 1276	0.19	0.4	HIP
00271−3634	HIP 2136	0.18	0.5	HIP
00406−4831	HIP 3186	0.04	0.8	HIP
00457−6752	HIP 3579	0.08	2.6	HIP
01043−5741	SUB 1 Aa,Ab	0.22	0.7	HIP
01180−4809	HIP 6075	0.32	1.5	HIP
01376−0223	RST4181 BC	0.15	0.0	WDS
02050−3748	HIP 9713	0.34	3.1	HIP
02065+0002	HIP 9827	0.05	2.3	REF
02143−4952	HIP 10421	0.08	0.0	HIP[b]
02442−5234	HIP 12775	1.33	4.4	REF
02466−3232	HIP 12954	1.33	3.8	HIP
02595−6415	HIP 13935	0.51	4.6	HIP
03274−4113	HIP 16097	0.17	2.6	HIP
03405+0508	STF 430 Aa,Ab	0.20	3.0	REF
03476−3625	KPP2826 Aa,Ab	0.45	3.2	HIP
03566−3313	HIP 18457	0.09	0.2	HIP
04157−5631	UC 1144 Aa,Ab	0.19	2.3	HIP
04249−3445	DAM1313 Aa1,Aa2	0.06	1.8	REF
05222−3218	HIP 25085	0.07	2.6	HIP
06203−3004	1 CMa	0.04	0.0	SB
06225−6342	HIP 30310	0.33	0.1	HIP
06237−3319	HIP 30410	0.07	0.1	HIP[b]
06357−7006	HJ 3885 Aa,Ab	0.13	2.0	WDS
06404−8223	HIP 31931	1.66	2.5	HIP
06460−6624	HIP 32414 AB	0.31	3.1	HIP
06460−6624	HIP 32414 BC	0.13	0.2	HIP[b]
07165−5513	HIP 35203	0.17	1.6	HIP[b]
07343−4517	HIP 36818	0.09	3.0	HIP
07480−1924	B 1077 Ba,Bb	0.12	0.7	WDS
07548−6613	HIP 38645	0.06	0.0	HIP[b]
08032−5401	HIP 39391	0.96	2.7	HIP[b]
08134−4534	HIP 40269	0.04	0.0	HIP[b]
08170−3525	HIP 40569	0.38	4.3	HIP
08422−6852	HIP 42709	0.67	1.8	HIP
08507−3825	JSP 308 Aa,Ab	0.14	2.7	WDS
09012+0157	CRC 57 Aa,Ab	0.19	1.3	MSC
09086−2960	HIP 44868	1.68	5.3	HIP
09350−7804	KOH 85 AC	1.80	4.7	WDS
09448−3633	HIP 47808	0.30	3.4	HIP
09538−6719	HIP 48528	0.36	3.2	HIP[b]
09589−5000	HIP 48928 AB	1.37	1.9	HIP[b]
09589−5000	HIP 48928 Aa,Ab	0.06	0.0	HIP[b]
10152−5846	HU 1596 BC	0.23	2.4	WDS
10212−1736	HIP 50701	1.08	3.4	HIP
10231−5032	HIP 50861	1.06	3.6	HIP[b]
10343−7807	HIP 51748	3.39	7.2:	HIP
10377−1103	HIP 52023	0.44	3.6	HIP[b]
10560−0254	HIP 53443	0.10	1.8	HIP[b]
11177+2722	HIP 55170	0.07	1.4	REF
11415−7703	HIP 57027	0.09	0.1	REF
11428−3549	HIP 57129	1.26	2.5	HIP
11515−2138	HIP 57827	0.11	1.2	HIP[b]
11565−5046	HIP 58226	0.75	3.1	HIP[b]
12114−1647	S 634 Aa,Ab	0.023	0.7	SB
12407−4803	HIP 61868	0.06	1.7	HIP[b]
12556−6900	HDS1813Aa,Ab	0.05	1.6	HIP
13103−3248	HIP 64264	1.78	3.6	HIP[b]
13240−5253	HIP 65385 AB	1.70	2.0	HIP
13240−5253	HIP 65385 Aa,Ab	0.29	0.3	HIP
13372−2337	HIP 66433	0.28	3.7	REF
14062−6543	SKF 107 Aa,Ab	0.98	3.6	HIP
14079−3736	HIP 69026	0.29	4.5	HIP
14219−3609	HIP 70214	1.09	3.9	HIP
14333−2707	HDS2056 Ba,Bb	0.05	0.2	HIP[b]
14333−3054	HIP 71162	0.24	3.2	HIP[b]
14336−0956	HIP 71188	1.28	3.3	HIP
14347−3528	HIP 71289	0.08	0.1	REF
14386−0710	HIP 71600	0.44	4.2	HIP[b]
14397−0957	HIP 71685	1.48	4.1	HIP
15031−4200	B 1257 BC	0.15	0.8	MSC
15031−4237	WIS 279 Aa,Ab	0.25	2.0	HIP[b]
15107−4344	CPO 415 Aa,Ab	1.39	5.1	REF
15594−3020	HIP 78313	0.65	2.5	HIP
16103−2209	HIP 79244	0.03	0.6	REF[b]
16358−5345	KPP3002 Aa,Ab	1.17	2.6	HIP[b]
16486−3715	HIP 82272	0.84	5.8	REF
16520−3602	HIP 82521 AB	0.39	1.5	HIP
16520−3602	HIP 82521 Aa,Ab	0.09	0.9	HIP
17522−2440	HIP 87453	2.65	6.1	HIP
18431+0742	LDS 1013 BC	0.39	0.9	MSC
18568−3002	KPP4129 Aa,Ab	0.13	2.0	HIP[b]
20363−1856	TOK 339 Aa,Ab	1.67	2.4	HIP
20516−2927	HIP 102963	1.49	5.3	HIP[b]
22247−6537	HIP 110630	0.14	3.1	REF[b]
22374−4550	SKF 384 Aa,Ab	0.21	4.0	HIP[b]
22419−3155	HIP 112064	0.12	0.0	HIP[b]
23232−5441	HIP 115455	1.62	2.6	HIP[b]
23257−4537	HIP 115648	0.26	2.4	HIP[b]
23308−4724	HIP 116045	0.23	2.4	HIP[b]

[a] HIP – *Hipparcos* suspected binary; MSC – multiple system; REF – reference star; SB – spectroscopic binary; WDS – neglected pair.
[b] Confirmed.

Table 4 highlights the 90 first-time resolutions of double stars or new subsystems by listing their approximate separations at discovery time, magnitude differences (mostly in the I band), and the corresponding observing programs. Full measurements of these pairs are found in the Table 2. Most new pairs (66) are *Hipparcos* suspected binaries. We also resolved serendipitously

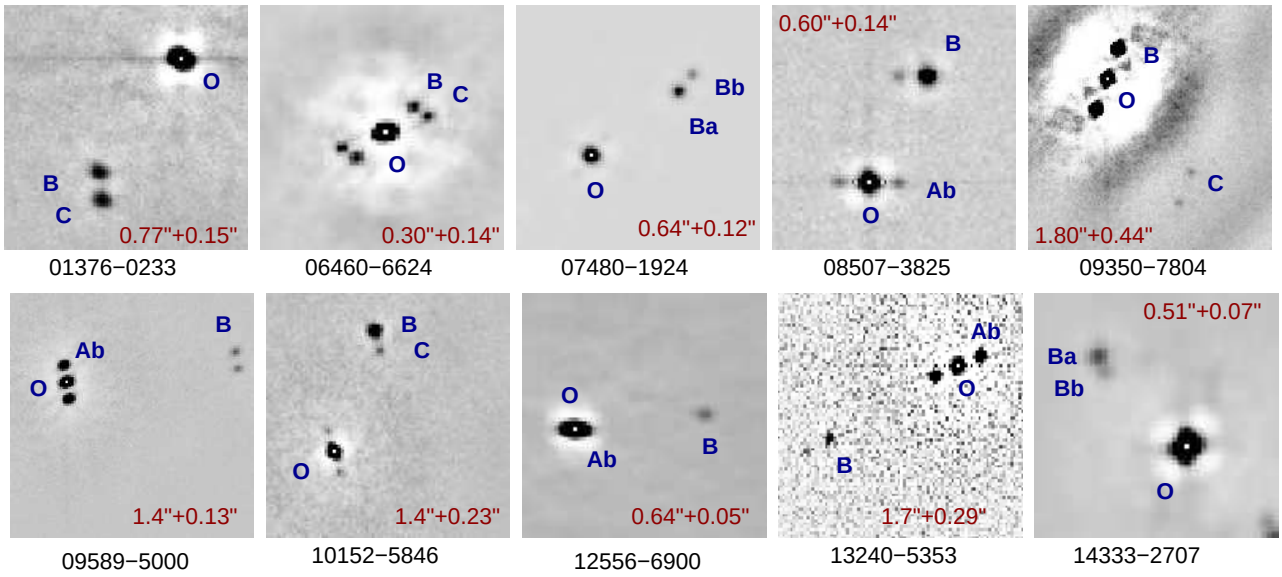

FIG. 2.— Triple systems discovered in 2019. Fragments of the speckle ACFs in arbitrary negative intensity scale are shown. The peaks corresponding to the components are marked, the central peak (white dot at coordinate origin) is labeled O. Separations of the wide and close pairs in arcseconds indicate the spatial scale.

12 reference stars. Seven subsystems in the previously known WDS pairs, also discovered accidentally, have the program code WDS. New resolutions are either very tight pairs or wider pairs with a large contrast; all "easy" pairs with comparable components and large separations were already discovered, e.g. by *Hipparcos*.

As in previous papers of this series, we discovered new visual multiple systems with three or more resolved components. This information will be ingested into the current version of the multiple-star catalog, MSC (Tokovinin 2018b). In the case of HIP 48928 (J09589−5000) and HIP 65385 (J13240−5253), both inner and outer pairs are new discoveries. Figure 2 presents fragments of the speckle ACFs of some multiple systems. Three new wide and faint companions to previously known closer pairs (J03302−7024, J09350−7804, and J09589−500) are optical, as revealed by *Gaia* DR2 by their discrepant proper motions and/or parallaxes. Similarly, the known 4.″2 pair SKF 107 (J14062−6543) is optical, while the chance of the new 1″ pair being physical is higher.

New tight binaries are promising candidates for orbit determination. HIP 79244 (J16103−2209) shows fast motion during one year. The bright spectroscopic binary HIP 30122 (J06203−3004, 1 CMa) with a period of 675 days was observed on request by J. Docobo and securely resolved into a 35-mas near-equal pair. Its single-lined spectroscopic orbit should be upgraded to a double-lined one to allow measurement of the orbital parallax.

3.3. *New and updated orbits*

Speckle measurements at SOAR are used to compute new and improve previously known orbits. The well-known difficulties inherent to visual binaries (insufficient coverage, inaccurate or misleading measures) resulted in the large number of poor-quality orbits in the general orbit catalog, VB6 (Hartkopf, Mason & Worley 2001). The situation is improving as new, substantially more accurate data become available. At the same time, many first-time orbits just computed from recent observations are tentative (grades 4 or 5) and contribute to the pool of poor orbits in the catalog as the older orbits become better known. In some cases, the lack of coverage leaves long-period orbits poorly constrained despite good modern measures. Nevertheless, even tentative (and possibly wrong) orbits are useful in several ways: as a synthesis of all existing data, for predicting binary positions and planning future measurements, etc.

In Table 5, orbital elements and their errors are given for 93 pairs observed in 2019. Formal grades and references to previous orbits are given in the last columns (SOAR2019 for the orbits computed here). Asterisks mark orbits where radial velocities from the literature are used jointly with position measures. The complementary Table 6 lists 34 provisional, poorly constrained orbits of grades 4 and 5 without errors, which in this case are large or even misleading. For circular and/or face-on orbits, some Campbell elements become degenerate and they are fixed accordingly. Some reliable orbits of grades 3 or better resulting from our work were already published in the Information Circulars (e.g. Tokovinin 2019). However, the Circulars do not provide errors of the elements, so we publish these orbits here with errors to give the full result (some with a slight adjustment using the latest measures). Orbit correction is a continuous process. Note that Table 5 also contains 25 orbits of excellent quality (grades 1 and 2). The official grades consider several factors (see Hartkopf, Mason & Worley 2001) and are not uniquely correlated with errors of the elements. For this reason, 16 low-grade orbits with reasonably small errors are kept in Table 5.

The orbital elements and their errors were determined by the weighted least-squares fit using the IDL program `ORBIT` (Tokovinin 2016b). We adopt weights proportional to σ^{-2}, where the errors σ are assigned according to the measurement technique (e.g. from 2 to 5 mas for speckle interferometry with 4-m class telescopes, 10 mas for *Hipparcos*, 50 mas or larger for visual micrometer measures) and corrected iteratively to reduce the impact of outliers, if necessary. In some cases the published radial velocities (RVs) are used, leading to the combined spectro-interferometric orbits. Mass sums are computed as a sanity check, especially helpful for poorly

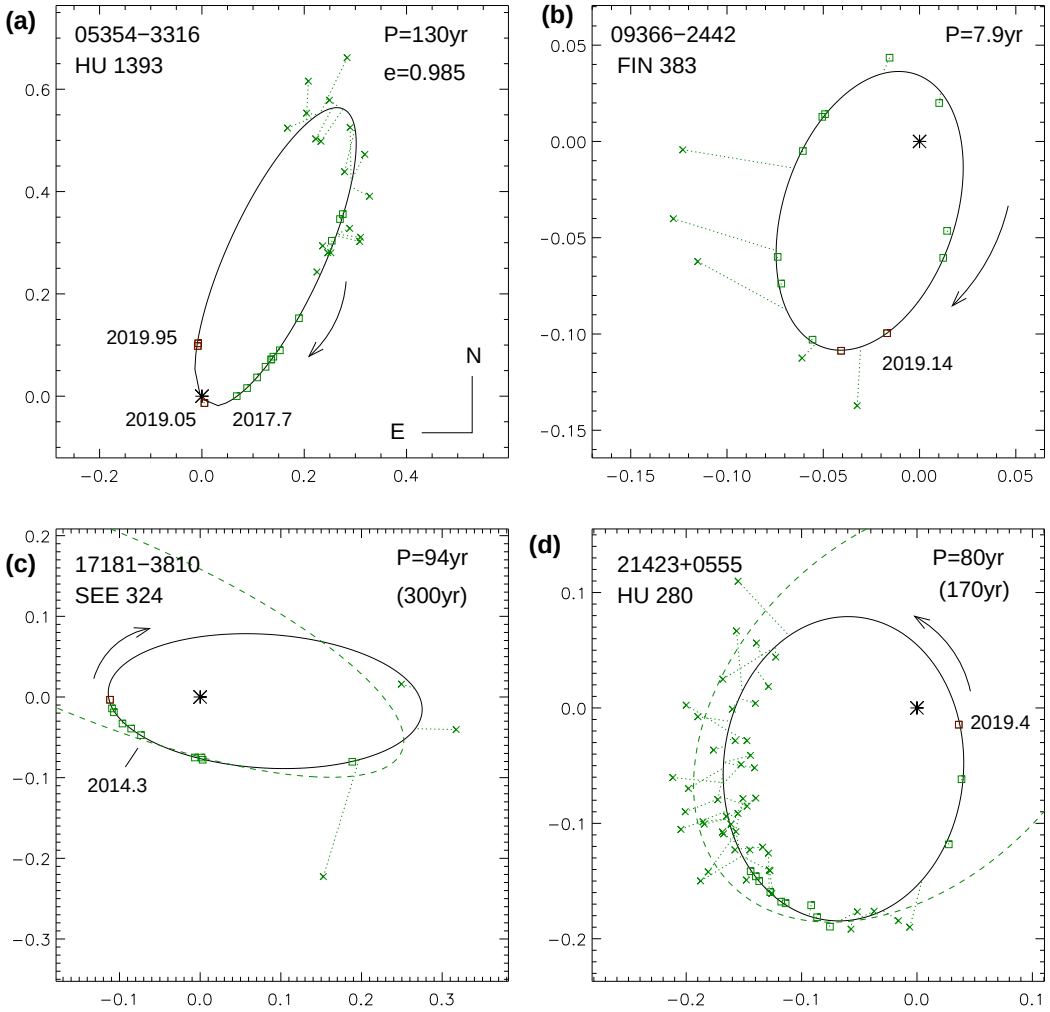

FIG. 3.— Orbits of "classical" visual binaries observed at SOAR in 2019. In this and following Figures, the axis scale is in arcseconds, the primary component (asterisk) is located at the coordinate origin. Green squares denote accurate speckle-interferometric measures of the secondary component (the 2019 measures are highlighted in red), crosses denote less accurate micrometer measures. The measures are connected to the orbit (ellipse) by short dotted lines. In the two lower panels, the dashed lines are previous orbits.

constrained preliminary orbits. Two pairs (J04303+1950 and J05229−4219) were unresolved in 2019 despite predictions of their previous orbits. These non-resolutions are accounted for by the new, corrected orbits.

Figure 3 gives four noteworthy examples where our observations substantially contributed to the knowledge of orbits of classical visual binaries. Speckle monitoring of J05354−3316 at SOAR (panel a) indicated diminishing separation, and in 2019 the pair passed through the periastron. In 2019.05 it was unresolved; however, the elongated power spectrum was fitted with a fixed $\Delta y = 1.3$ mag, yielding a separation of 15 mas (below the diffraction limit). Two good measures were taken after periastron. The extremely high eccentricity of $e = 0.985 \pm 0.002$ is well constrained by our data. If the periastron had been missed, we would have to wait for 130 years for the next one. The case of J09366−2442 in panel (b) shows how unreliable or even misleading the visual measures of close pairs can be. Including these measures in the orbital fit would spoil the result, while the speckle data alone define the orbit quite well. The period of J17181−3810 (panel c) was revised from 300 to 94 yr. This pair was not observed at all for 69 years, from 1897 till 1966, which is rather unusual. Based on three micrometer measures and only a few speckle data available in 2014, the previous 300 yr orbit by Tokovinin et al. (2015) was just a bold guess! Now the elements are constrained better, but the long period means that this orbit will remain poorly known for decades. Yet another case of radical orbit revision (from 170 to 80 yr) is J21423+0555 (panel d). This pair now rapidly moves through the periastron and in a few more years its eccentric orbit will become definitive.

To illustrate the impact of SOAR observations on the knowledge of stellar masses, we plot in Figure 4 four well-constrained orbits of nearby M-type dwarfs, continuing the work of Mason et al. (2018). Full analysis of mass-luminosity relation is outside the scope of this paper, and the orbits are highlighted here only to illustrate the potential of HRCam data in this area. The spectral types in the Figure are retrieved from Simbad. All orbits except the last one were known previously, but with a lower accuracy. For example, for J10367+1522 (DAE 3 BC) Calissendorff et al. (2017) found an excess of mass which is not confirmed by our new orbit, constrained nicely by the 2019 measure. This is a triple system of M dwarfs at 20 pc where the outer orbit is also computed, although it is still poorly constrained. In con-

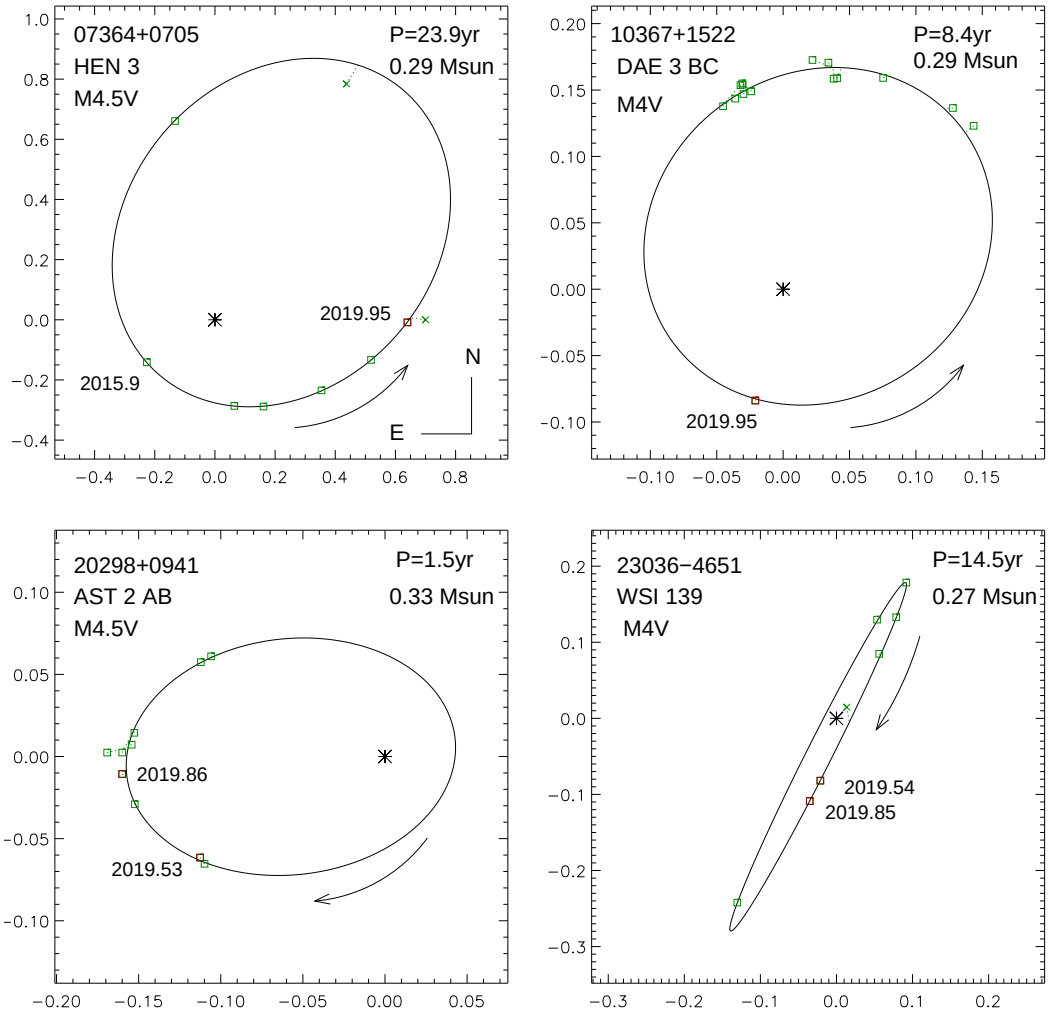

FIG. 4.— New orbits of four M4V dwarf binaries. The mass sum computed from the orbital elements and parallax is indicated.

trast, J20298+0941 (GJ 791.2), previously listed in the WDS as a tight visual triple AB+AC, is in fact a simple binary, never resolved as triple at SOAR or elsewhere; another companion D at 9″ is optical. We used the RVs and position measures by Benedict et al. (2016) to get a well-constrained combined orbit. The RVs, however, are likely biased because the resulting orbital parallax of 93±3 mas contradicts the accurate parallax measured by the same authors (113.4±0.2 mas), while the mass ratio of 0.5 inferred from the RV amplitudes contradicts $\Delta J = 2.3$ mag measured at SOAR. The *Gaia* parallax, 133.8±1.4 mas, is obviously biased by the orbit. The last pair of M-dwarfs in Figure 4, J23036−4651 (WSI 139), did not have previous orbit determinations. Nevertheless, its 14.5 yr orbit based almost entirely on the SOAR data is already quite reliable; the rms residuals are 2 mas.

Figure 5 illustrates the emerging combined spectro-interferometric orbit of J05066−7736 (HIP 23776). Astrometric orbit with a period of 1.9 yr based on *Hipparcos* was published by Goldin & Makarov (2006). Our orbit with a period of 2.18 yr and a semimajor axis of 53.1±0.9 mas is strongly constrained by three measures taken in 2019. All measures come from SOAR, and the rms residuals to the orbit are 1.1 mas. High-resolution spectroscopy (to be reported elsewhere) yields RV measurements of both components. The preliminary orbital parallax is 26.4±1.1 mas and the masses are 0.89 and 0.83 solar. The *Gaia* parallax is 28.68±0.18 mas. Continued speckle interferometry and spectroscopy of this pair during another year will lead to accurate mass measurement. The spectral type G8VFe-1.6CH-1.2 suggests chemical peculiarity, while the fast proper motion of 0.″45 yr^{-1} is typical of halo or thick disk stars. Nordström et al. (2004) measured the metallicity [Fe/H] of −0.47 and determined the mass ratio of 0.89±0.01; our preliminary orbit gives the mass ratio of 0.93±0.01.

TABLE 5
VISUAL ORBITS

WDS *HIP*	Discov.	P (yr)	T (yr)	e	a (arcsec)	Ω (deg)	ω (deg)	i (deg)	Grade	Ref.[a]
00121−5832	RST4739	36.91	1989.95	0.597	0.236	55.0	278.2	147.4	3	Tok2019h
975		±0.45	±0.18	±0.026	±0.006	±6.8	±5.7	±3.6		
00277−1625	YR 1 Aa,Ab	13.35	2014.41	0.024	0.1208	167.8	270.3	69.6	4	Tok2019h

TABLE 5
Visual orbits

2190		±0.15	±0.54	±0.019	±0.0020	±0.8	±14.8	±0.9		
00462−2214	RST4155	49.27	2003.49	0.305	0.1693	177.9	141.7	138.0	2	Hei1984a
3606		±1.13	±0.53	±0.022	±0.0044	±4.3	±2.5	±2.3		
00550−5315	RST 23	140	1973.59	0.85	0.569	182.3	79.4	105.9	4	SOAR2019
...		±19	±1.62	±0.09	±0.152	±5.0	±4.5	±5.7		
01308−5940	TOK 183	6.586	2020.432	0.455	0.0671	352.3	42.4	93.5	3	Tok2015c
7040		±0.059	±0.079	±0.017	±0.0013	±0.6	±2.8	±0.8		
02038−0020	TOK 38 Aa,Ab	5.660	2005.426	0.367	0.0377	271.9	30.5	71.7	3	SOAR2019*
9631		±0.006	±0.020	±0.006	±0.0009	±2.1	±1.0	±3.8		
02290−1959	RST2280 Aa,Ab	31.41	2020.69	0.686	0.557	185.2	38.7	154.1	3	Tok2018i
11565		±0.24	±0.07	±0.014	±0.012	±8.4	±8.8	±3.2		
02305−4342	ELP 1 Aa,Ab	14.42	2020.0	0.032	0.130	122.3	14.7	139.7	3	Tok2018c
...		±1.36	±5.2	±0.017	±0.008	±5.5	±133.6	±4.1		
02517−5234	HU 1562	67.62	2019.94	0.950	0.2588	49.1	168.9	128.9	3	Tok2019h
13341		±1.07	±0.17	±0.022	±0.0036	±3.5	±6.8	±11.5		
03271+1845	CHR 10 AB	16.88	1994.4	0.040	0.0787	91.2	206.7	42.8	3	Ole1999
16077		±0.10	±3.3	±0.032	±0.0066	±5.6	±66.1	±6.9		
03379+0538	YSC 27	16.51	2013.025	0.222	0.1399	98.6	94.7	123.5	3	Cve2017b
16390		±0.20	±0.066	±0.012	±0.0015	±1.1	±1.7	±0.7		
03462−2423	RST2321	96.26	2013.99	0.832	0.2150	11.5	155.8	43.9	3	SOAR2019
17600		±2.43	±0.40	±0.027	±0.0034	±9.6	±10.9	±4.6		
04008+0505	A 1937	46.08	2014.74	0.535	0.0974	31.9	0.4	40.8	2	Tok2019h
18374		±1.04	±0.12	±0.008	±0.0014	±3.0	±3.4	±2.0		
04063+1952	BAG 4	15.89	2012.25	0.921	0.0959	133.6	266.4	114.0	3	Bag2001
...		±0.12	±0.39	±0.010	±0.0025	±8.6	±2.7	fixed		
04070−1000	HDS 521 AB	21.04	2017.938	0.712	0.2302	220.4	77.4	121.5	2	Tok2019h
19206		±0.04	±0.025	±0.004	±0.0020	±0.4	±0.3	±0.5		
04142−4608	RST2338	18.145	2002.715	0.631	0.1941	169.1	138.9	30.6	2	Doc2016i
19758		±0.054	±0.088	±0.012	±0.0021	±5.8	±6.5	±1.4		
04303+1950	PAT 10	11.016	1986.577	0.754	0.1280	127.6	34.1	142.1	4	SOAR2019*
21008		±0.020	±0.040	±0.007	±0.0019	±2.6	±3.0	±2.0		
04318−2407	RST2347	122.9	2010.87	0.523	0.1734	163.5	339.7	129.4	3	Tok2019h
21133		±8.2	±0.44	±0.025	±0.0065	±4.5	±5.8	±4.6		
04389−1207	HDS 599	50.13	2004.18	0.817	0.3174	153.9	281.2	76.5	3	Tok2019h
21644		±1.45	±0.30	±0.018	±0.0155	±1.0	±1.0	±0.9		
04406−0912	WOR 17	215.5	1994.0	0.813	1.919	11.7	36.7	32.3	5	SOAR2019
21765		±20.8	±0.35	±0.014	±0.086	±4.6	±5.1	±3.4		
04539−2032	HDS 633	11.834	2018.197	0.913	0.1429	167.6	157.9	56.0	3	Tok2019d
22772		±0.107	±0.072	±0.013	±0.0042	±5.4	±9.1	±3.1		
04553−0352	RST4257 AB	87.63	2011.40	0.566	0.2497	169.8	3.1	119.5	4	SOAR2019
...		±2.48	±0.74	±0.023	±0.0142	±2.9	±4.7	±3.2		
05066−7734	TOK 785	2.178	2020.088	0.181	0.0531	284.5	7.0	60.6	3	SOAR2019*
23776		±0.018	±0.034	±0.014	±0.0009	±1.4	±6.5	±2.2		
05069−2135	DON 93 BC	115.4	2002.63	0.339	1.209	89.6	257.6	150.0	4	SOAR2019
...		±3.1	±0.45	±0.030	±0.016	±4.7	±5.6	±3.5		
05229−4219	TOK 93 Aa,Ab	5.99	2013.78	0.555	0.0625	238.2	93.4	64.4	3	Tok2016e
15148		±0.12	±0.12	±0.036	±0.0031	±2.8	±1.1	±2.5		
05245−0224	MCA 18 Aa,Ab	9.414	2011.046	0.361	0.0472	125.3	12.6	103.5	2	Tok2015c
25281		±0.041	±0.250	±0.018	±0.0016	±1.3	±9.3	±1.8		
05272+1758	MCA 19 Aa,Ab	15.914	2014.60	0.806	0.0757	251.9	317.1	109.4	2	Jte2018
25499		±0.073	±0.16	±0.083	±0.0036	±1.7	±5.6	±7.3		
05354−3316	HU 1393	130.0	2019.04	0.985	0.6590	205.9	73.7	113.5	3	FRM2014a
26245		±4.0	±0.030	±0.002	±0.0515	±1.4	±1.5	±1.8		
05365+2556	CHR 203	13.56	1993.65	0.947	0.0848	135.9	50.0	160.0	3	SOAR2019
26322		±0.126	±0.299	±0.010	±0.0181	±9.4	fixed	±53.7		
06035+1941	MCA 24	13.061	2006.52	0.808	0.0555	224.4	291.5	111.8	2	Msn1997a
28691		±0.031	±0.16	±0.045	±0.0022	±3.3	±9.2	±7.8		
06138−2352	JNN 50 Ba,Bb	11.75	2020.36	0.74	0.263	18.8	295.4	120.7	4	SOAR2019
29568		±1.03	±0.23	±0.12	±0.020	±12.5	±9.5	±2.1		
06146−0434	CHR 164 Aa,Ab	18.94	2017.28	0.762	0.0491	287.4	227.1	57.8	3	Tok2019d
29629		±0.64	±0.29	±0.037	±0.0046	±7.0	±12.1	±6.1		
06253+0130	FIN 343	76.76	2020.49	0.360	0.1321	165.3	153.7	161.9	3	Tok2019d
30547		±3.22	±0.45	±0.014	±0.0023	±21.8	±26.9	±4.6		
06573−4929	RST5253 AB	50.66	2006.36	0.038	0.2170	148.8	87.5	72.2	3	Hrt2012a
33455		±1.53	±2.03	±0.032	±0.0041	±0.6	±15.2	±0.7		
07312+0210	TOK 393	5.71	2015.83	0.094	0.0606	27.3	168.4	144.2	3	Tok2017c
36557		±0.14	±0.25	±0.030	±0.0026	±7.8	±19.7	±5.5		
07364+0705	HEN3	23.93	2016.208	0.587	0.6402	85.7	57.8	14.4	4	Tok2018e
...		±0.40	±0.008	±0.005	±0.0051	±6.2	±6.4	±1.6		
07560+2342	COU 929	45.09	1997.98	0.4746	0.2555	186.70	70.66	71.86	1	Hrt2009
38755		±0.19	±0.21	±0.0034	±0.0011	±0.23	±0.73	±0.22		
08125−4616	CHR 143 Aa,Ab	33.08	2017.67	0.284	0.0723	172.7	253.5	69.9	3	Tok2015c
40183		±0.46	±0.18	±0.015	±0.0010	±1.0	±2.7	±1.1		
08158−1027	RST3578 AB	29.37	2017.413	0.470	0.2220	93.3	216.8	59.3	3	Tok2019d
40465		±0.09	±0.076	±0.019	±0.0043	±1.1	±2.4	±1.7		
08230−7102	HDS1196	19.45	2021.85	0.63	0.0652	16.3	175.7	133.6	3	SOAR2019
41093		±1.72	±1.33	±0.25	±0.0079	±18.6	±32.2	±24.5		

TABLE 5
Visual orbits

08255−4058	RST3592	133.8	2009.420	0.512	0.1442	165.0	246.2	140.4	3	SOAR2019
...		±19.2	±0.46	±0.050	±0.0179	±10.8	±11.8	±11.1		
09252−1258	WSI 73	12.715	2018.157	0.627	0.1294	93.1	42.7	85.9	4	Tok2017b
46191		±0.123	±0.059	±0.009	±0.0025	±0.5	±2.0	±0.4		
09366−2442	FIN 383	7.883	2017.428	0.638	0.0814	176.2	223.7	130.9	2	Tok2018b
47159		±0.041	±0.037	±0.011	±0.0020	±2.9	±3.8	±2.3		
09439−5738	HDS1404 Aa,Ab	21.55	2019.79	0.723	0.1345	165.2	4.2	59.0	3	SOAR2019
47736		±0.835	±0.050	±0.018	±0.0108	±3.5	±5.6	±2.9		
09442−2746	FIN 326	18.390	2020.924	0.506	0.1075	175.0	138.2	126.8	2	Doc2013d
47758		±0.086	±0.088	±0.015	±0.0012	±1.8	±2.6	±0.9		
09474+1134	MCA 34 AB	15.203	2003.96	0.3129	0.11097	203.09	22.3	76.26	2	Jte2018
48029		±0.019	±0.11	±0.0065	±0.00084	±0.50	±2.8	± 0.49		
10116+1321	HU 874	17.974	2003.819	0.928	0.1528	111.6	317.9	82.4	2	Hrt1996a
49929		±0.032	±0.092	±0.006	±0.0055	±0.6	±2.6	±0.8		
10345−3721	RST3706	62.6	2025.8	0.292	0.1517	40.8	324.1	103.9	3	SOAR2019
51760		±6.343	±1.773	±0.092	±0.0183	±2.1	±17.3	±2.3		
10367+1522	DAE 3 BC	8.427	2011.326	0.358	0.1382	104.1	44.4	21.4	4	Jnn2017b
...		±0.029	±0.041	±0.009	±0.0030	±10.5	±10.2	±3.8		
10373−4814	SEE 119	16.672	2019.819	0.771	0.3999	35.7	287.0	123.3	2	Tok2019d
51986		±0.032	±0.005	±0.003	±0.0021	±0.4	±0.3	±0.3		
10397−3755	HDS1523	59.7	2018.40	0.698	1.014	8.0	55.5	132.5	3	SOAR2019
52190		±1.24	±0.002	±0.003	±0.015	±0.6	±0.5	±0.6		
11053−2718	FIN 47 AB	7.612	2013.749	0.370	0.1346	45.1	156.5	94.0	2	Jte2018
54204		±0.007	±0.088	±0.013	±0.0015	±0.4	±3.9	±0.4		
11235+0701	BAG 24 Aa,Ab	20.810	2014.412	0.300	0.2275	150.0	222.0	160.0	3	SOAR2019
55605		±0.074	±0.209	±0.018	±0.0016	±16.8	±18.9	fixed		
11446−4925	RST9004 AB	35.43	2009.866	0.409	0.3074	139.0	350.1	27.5	2	Wol2014
57269		±0.13	±0.029	±0.003	±0.0014	±1.8	±1.9	±0.8		
12463−6806	R 207 AB	188.0	1874.2	0.79	1.16	138.6	72.5	53.3	3	FMR2012g
62322		±16.5	±6.5	±0.13	±0.23	±12.1	±11.3	±9.9		
13190−2536	HDS1866	22.72	2008.29	0.397	0.1435	18.3	225.8	137.8	3	SOAR2019
64970		±0.37	±0.16	±0.024	±0.0032	±5.0	±5.4	±2.6		
13317−0219	HDS1895	3.239	2013.781	0.534	0.0968	309.2	358.8	19.6	1	Hrt2012a*
659820		±0.002	±0.006	±0.006	±0.0007	±2.7	±3.0	±2.3		
13334+0919	HDS1902	26.15	2008.55	0.54	0.131	124.3	309.0	27.7	3	SOAR2019
66132		±0.51	±0.44	±0.01	±0.016	±34.2	±34.5	±15.9		
13396+1045	BU 612 AB	22.532	2019.7346	0.5422	0.19932	36.71	356.9	45.34	1	Msn1999a
66640		±0.020	±0.0023	±0.0023	±0.00050	±0.61	±1.1	±0.37		
13520−3137	BU 343 AB	254.8	1996.36	0.646	1.0709	187.2	242.9	135.4	3	Tok2014a
67696		±4.8	±0.09	±0.005	±0.0100	±0.6	±0.9	±0.4		
13598−0333	HDS1962	9.764	2008.366	0.405	0.0785	34.6	235.3	57.0	2	Tok2018i
68380		±0.078	±0.075	±0.014	±0.0016	±1.6	±2.3	±1.2		
14025−2440	B 263 AB	205.9	2011.84	0.533	0.597	19.8	65.5	48.8	4	Tok2015c
68587		±17.8	±0.64	±0.024	±0.037	±1.6	±4.8	±1.7		
14035+1047	GJ 538	9.876	2011.177	0.480	0.3156	74.0	183.0	96.9	3	SOAR2019*
68682		±0.002	±0.005	±0.001	±0.0006	±0.1	±0.2	±0.2		
14382+1402	TOK 406	8.29	2016.044	0.373	0.0998	7.3	168.3	130.5	3	Tok2018e
71572		±0.14	±0.028	±0.010	±0.0013	±1.4	±2.0	±1.0		
14581−4852	WSI 80	22.39	2020.52	0.791	0.4015	86.6	109.2	108.4	3	Tok2015c
73241		±2.08	±0.19	±0.061	±0.0108	±3.6	±1.1	±0.5		
16059+1041	HDS2273 Aa,Ab	33.00	1992.977	0.426	0.3512	160.6	234.6	35.1	3	Tok2019h
78864		±0.13	±0.055	±0.004	±0.0021	±1.2	±0.9	±0.9		
16534−2025	WSI 86	14.91	2014.96	0.502	0.2697	13.1	26.7	132.0	4	SOAR2019
82621		±0.25	±0.17	±0.013	±0.0059	±3.0	±5.9	±2.3		
17156−1018	BU 957	91.1	2030.2	0.570	0.287	25.0	28.8	101.1	2	Tok2015c
84423		±2.9	±1.8	±0.048	±0.013	±1.2	±4.2	±1.1		
17181−3810	SEE 324	94.2	2020.54	0.414	0.195	266.3	179.9	117.8	3	Tok2015c
84634		±12.3	±1.55	±0.028	±0.007	±1.9	±14.1	±3.0		
17240−0921	RST3972 Aa,Ab	15.262	2006.017	0.570	0.1465	69.2	16.8	25.5	2	Sod1999
85141		±0.018	±0.038	±0.004	±0.0012	±3.5	±3.9	±1.8		
17415−5348	HDS 2502	20.39	2018.044	0.594	0.1341	158.5	321.5	136.7	3	Tok2017c
86569		±0.34	±0.028	±0.008	±0.0010	±1.6	±2.1	±1.3		
17586−1306	HU 190	162.7	2011.40	0.422	0.3700	15.4	0.0	180.0	4	Tok2019h
88010		±12.3	±0.66	±0.027	±0.0142	±3.2	fixed	fixed		
18480−1009	HDS2665	38.44	2023.47	0.411	0.4796	36.4	195.7	56.4	4	Tok2016e
92250		±1.22	±0.30	±0.038	±0.0058	±2.4	±5.5	±0.7		
20048+0109	TOK 699	7.83	2018.578	0.241	0.1579	74.1	45.1	36.3	3	Tok2018i
98878		fixed	±0.037	±0.008	±0.0030	±3.8	±3.6	±2.0		
20210−1447	BLA 7 Aa,Ab	3.762	2015.642	0.452	0.0487	43.6	124.2	75.1	2	Tok2015c
100325		±0.000	±0.009	±0.009	±0.0010	±1.3	±1.0	±2.0		
20298+0941	AST 2 AB	1.4708	2019.185	0.573	0.1118	287.7	20.4	148.5	3	Tok2019h*
...		±0.0004	±0.009	±0.010	±0.0015	±2.4	±3.6	±3.0		
20462+1554	WSI 110 Aa,Ab	4.871	2003.255	0.254	0.0979	143.6	344.0	78.5	3	SOAR2019*
102490		±0.001	±0.018	±0.006	±0.0015	±1.0	±1.5	±1.5		
21088−0426	HDS3013 Aa,Ab	25.019	2019.391	0.557	0.3138	153.1	99.3	134.9	3	Tok2018e
104383		±0.026	±0.017	±0.007	±0.0019	±1.5	±1.1	±0.7		
21094−7310	I 379 AB	5.389	2017.555	0.690	0.1829	194.4	183.4	93.3	2	SOAR2019

TABLE 5
Visual orbits

104440		±0.059	±0.041	±0.022	±0.0040	±0.5	±3.9	±1.5		
21130−1133	VOU 24 AB	128.5	2020.03	0.321	0.264	65.3	250.0	161.9	4	SOAR2019
...		±8.1	±1.93	±0.012	±0.017	±10.2	fixed	±12.4		
21198−2621	BU 271 AB	189.1	1841.48	0.631	2.159	244.7	190.5	65.2	3	Tok2019h
105312		±4.5	±4.06	±0.021	±0.013	±1.3	±3.8	±0.4		
21395−0003	BU 1212 AB	48.68	1972.09	0.867	0.4277	141.1	293.6	55.2	2	Tok2019h
106942		±0.34	±0.28	±0.009	±0.0093	±1.9	±1.6	±0.8		
21423+0555	HU 280	80.77	2020.46	0.721	0.1778	198.2	103.3	51.8	2	USN2006a
107153		±2.52	±0.15	±0.024	±0.0074	±4.9	±2.9	±2.2		
21477−3054	FIN 330 AB	20.218	2007.26	0.427	0.1240	31.9	215.2	108.4	2	Doc2013d
107608		±0.134	±0.16	±0.026	±0.0016	±1.2	±3.1	±0.9		
21522+0538	JOD 23 AB	9.08	2019.386	0.447	0.1406	163.7	0.0	0.0	4	Tok2019c
107948		±0.11	±0.024	±0.008	±0.0013	±1.2	fixed	fixed		
22056−5858	B 548	77.03	2019.8	0.186	0.265	210.9	54.0	73.0	3	SOAR2019
109060		±1.45	±3.9	±0.048	±0.006	±1.7	±23.1	±1.3		
22220−3431	B 557 Aa,Ab	107.97	2020.025	0.893	0.3559	190.0	72.8	112.6	3	Tok2019h
110419		±4.79	±0.133	±0.019	±0.0290	±1.9	±1.7	±2.4		
22342−1841	HU 389	186.0	2006.32	0.417	0.2995	122.5	158.9	50.6	3	Tok2019h
111406		±12.2	±1.24	±0.024	±0.0085	±2.6	±2.8	±1.7		
22474+1749	WSI 93	25.45	2017.372	0.634	0.2391	1.6	88.8	34.2	3	Tok2017c
112506		±1.27	±0.030	±0.014	±0.0083	±4.6	±5.5	±1.8		
22479−5705	B 2059	43.17	2007.00	0.70	0.125	71.9	176.0	102.1	3	SOAR2019
112561		±2.82	±2.70	fixed	±0.007	±4.4	±24.7	±3.7		
22532−3750	HDS3250 Aa,Ab	10.62	2011.77	0.28	0.1395	226.0	100.1	56.7	4	SOAR2019
113010		±1.51	±0.17	±0.13	±0.0053	±4.7	±12.4	±5.8		
23036−4651	WSI 139	14.50	2015.48	0.230	0.2572	153.3	162.4	93.8	3	SOAR2019
...		±2.15	±0.44	±0.059	±0.0257	±0.8	±14.7	±0.5		
23210+1715	WSI 11	7.95	2020.44	0.372	0.0852	163.7	22.9	28.7	3	Tok2017c
115288		±0.10	±0.18	±0.043	±0.0042	±16.8	±18.1	±10.1		

[a] References to VB6 are provided at http://ad.usno.navy/mil/wds/orb6/wdsref.txt

TABLE 6
Preliminary visual orbits

WDS	Discov.	P (yr)	T (yr)	e	a (arcsec)	Ω (deg)	ω (deg)	i (deg)	Grade	Ref.[a]
00325−6800	DON 7	150	2037.8	0.186	0.608	175.0	337.0	180.0	4	SOAR2019
00345−0433	D 2 AB	777	2008.5	0.79	1.111	83.1	270.4	77.6	4	Hrt2010a
02128−0224	TOK 39 Aa,Ab	0.2595	1989.5599	0.689	0.0144	241.0	74.3	30.0	3	SOAR2019*
03178−1407	HU 432	73.67	1979.23	0.152	0.2017	45.4	223.2	40.4	4	SOAR2019
05190−2159	RST2375	164.019	2015.515	0.326	0.3205	154.4	262.0	51.8	4	Hrt2011d
05505−5246	B 1493	113.0	2005.00	0.67	0.1625	247.9	170.2	140.5	4	SOAR2019
06515+0358	A 1956	110.9	2002.6	0.437	0.3705	67.2	354.5	115.1	4	SOAR2019
08342−0957	HDS1226	54.6	2003.13	0.386	0.203	202.6	113.6	119.5	4	SOAR2019
08582+1945	LDS3836	134.4	2006.25	0.661	3.234	38.5	91.0	20.0	5	SOAR2019
09074−4357	B 1646 AB	208	2029.4	0.60	0.188	15.9	161.1	116.2	4	SOAR2019
09077+1040	CHR 257	80.9	2030.06	0.55	0.201	106.2	170.7	79.2	3	SOAR2019
09370−2610	WSI 127	31.98	2010.47	0.0	0.3907	284.0	0.0	0.0	5	SOAR2019
09393−1013	RST3652	500	2002.254	0.70	1.355	277.7	96.1	113.7	5	SOAR2019
10038−0823	HDS1454	32.74	2010.60	0.70	0.087	177.9	334.6	124.8	4	SOAR2019
10193−1232	RST3688	180	2005.08	0.544	0.6852	142.1	278.5	80.9	4	SOAR2019
10476−1538	TOK 714 Aa,Ab	9.32	2015.59	0.103	0.0572	120.2	43.3	117.1	4	SOAR2019
11064−3545	DAW 132 AB	163.3	1983.62	0.97	1.199	121.8	177.4	141.2	5	SOAR2019
11342+1101	YSC 43 Aa,Ab	10.97	2005.44	0.522	0.0666	351.8	77.2	101.3	4	SOAR2019
11495−1636	TOK 717 Aa,Ab	24.0	2018.05	0.145	0.1984	292.5	108.2	102.6	4	SOAR2019
13327+2230	HDS1898	30.0	2001.8	0.82	0.3056	251.0	94.1	74.0	3	FMR2013d
13344−4224	SEE 182	480	2017.290	0.983	1.073	28.1	288.0	55.0	5	SOAR2019
13344−5931	TOK 403	18.44	2021.11	0.385	0.1441	77.2	265.5	117.7	4	SOAR2019
14038−6022	VOU 31 AB	182 0	2031.30	0.60	0.788	251.9	171.8	125.4	4	SOAR2019
15234−5919	HJ 4757	600	2111.7	0.404	1.275	123.9	218.7	127.8	4	Hrt2010a
16038+1406	HDS2265	53.7	2021.17	0.815	0.3544	1.3	153.1	63.6	4	Tok2018e
17012−1213	HU 163	160	2009.0	0.73	0.1994	154.7	28.6	93.8	4	SOAR2019
19197−2836	B 433 AB	250	2027.51	0.458	0.441	219.7	97.7	57.2	4	SOAR2019
19563−3137	TOK 698	13.0	2016.29	0.292	0.1063	59.8	44.0	90.8	4	SOAR2019
20521+0205	A 2286 AB	273.0	2015.07	0.687	0.311	83.3	226.8	60.6	4	SOAR2019
21477−1813	CHR 223	73.829	2025.728	0.311	0.1713	110.9	275.3	109.9	4	Tok2015c
21491−7206	HEI 598	120	2016.44	0.349	1.565	42.8	67.8	51.8	4	SOAR2019
22266−1645	SHJ 345 AB	3500	2020.45	0.913	14.558	289.1	158.4	34.3	4	Hle1994
22378−5004	HDS3214	82.7	2020.14	0.75	0.145	110.6	64.3	138.0	4	Tok2019d
22441+0644	TOK 703	5.02	2015.93	0.316	0.0585	168.7	166.5	134.3	4	SOAR2019

[a] References to VB6 are provided at http://ad.usno.navy/mil/wds/orb6/wdsref.txt

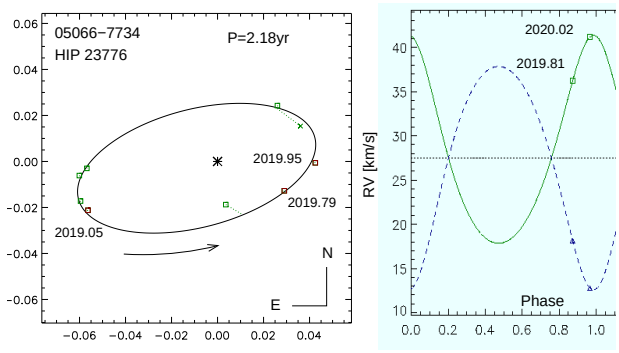

FIG. 5.— Combined preliminary spectro-interferometric orbit of HIP 23776.

4. SUMMARY

Continued monitoring of close visual binaries at SOAR results in gradual improvement of the orbits, especially for tight and nearby pairs with short periods like HIP 23776 (Figure 5). Good-quality visual orbits coupled to precise parallaxes from *Gaia* will vastly extend our knowledge of stellar masses. Knowledge of visual orbits is needed in various astrophysical contexts, for example for binaries hosting exoplanets.

The SOAR speckle program has resulted in the discovery of many new close binaries and subsystems. This list is extended here by the 90 new pairs, although *Gaia* reveals some wide and faint new companions as unrelated (optical). During 2019, the core program on visual multiples has been supplemented by various binary surveys like high-resolution follow-up of TESS exo-planet candidates and the multiplicity survey of Upper Scorpius association.

We thank the SOAR operators for efficient support of this program, and the SOAR director J. Elias for allocating some technical time. This work is based in part on observations carried out under CNTAC programs CN2019A-2 and CN2019B-13.

R.A.M. and E.C. acknowledge support from the Chilean Centro de Excelencia en Astrofísica y Tecnologías Afines (CATA) BASAL AFB-170002, and FONDECYT/CONICYT grant # 1190038.

This work used the SIMBAD service operated by Centre des Données Stellaires (Strasbourg, France), bibliographic references from the Astrophysics Data System maintained by SAO/NASA, and the Washington Double Star Catalog maintained at USNO. This work has made use of data from the European Space Agency (ESA) mission Gaia (https://www.cosmos.esa.int/gaia processed by the Gaia Data Processing and Analysis Consortium (DPAC, https://www.cosmos.esa.int/web/gaia/dpac/consortium Funding for the DPAC has been provided by national institutions, in particular the institutions participating in the Gaia Multilateral Agreement.

Facilities: SOAR.

REFERENCES

Benedict, G. F., Henry, T. J., Franz, O. G., et al. 2016, AJ, 152, 141
Calissendorff, P., Janson, M., Köhler, R., et al. 2017, A&A, 604,82
Gaia Collaboration, Brown, A. G. A., Vallenari, A., Prusti, T., et al. 2018, A&A, 595, 2 (Vizier Catalog I/345/gaia2).
Goldin, A. & Makarov, V. V. 2006, ApJS, 166, 341
Hartkopf, W. I., Mason, B. D. & Worley, C. E. 2001, AJ, 122, 3472
Hartkopf, W. I., Tokovinin, A. & Mason, B. D. 2012, AJ, 143, 42
Horch, E. P., van Belle, G. T., Davidson, J. W., Jr. et al. 2015, AJ, 150, 151
Horch, E. P., Casetti-Dinescu, D. I., Camarata, M. A., et al. 2017, AJ, 153, 212
Horch, E. I., Tokovinin, A., Weiss, S. A., et al. 2019, AJ, 157, 56
Mason, B. D., Wycoff, G. L., Hartkopf, W. I., et al. 2001, AJ, 122, 3466 (WDS)
Mason, B. D., Hartkopf, W. I., Miles, K. N., et al. 2018, AJ, 155, 215
Mendez, R. A., Claveria, R. M., Orchard, M. E., & Silva, J. F. 2017, AJ, 154, 187
Nordström, B., Mayor, M., Andersen, J., et al. 2004, A&A, 419, 989
Perryman, M. A. C., Lindegren, L., Kovalevsky, J. ey al. 1997, A&A, 323, L49
Tokovinin, A. 2012, AJ, 144, 56
Tokovinin, A. 2016a, AJ, 152, 138
Tokovinin, A. 2016b, ORBIT: IDL software for visual, spectroscopic, and combined orbits. Zenodo, doi:10.2581/zenodo.61119
Tokovinin, A. 2018a, PASP, 130, 5002
Tokovinin, A. 2018b, ApJS, 235, 6
Tokovinin, A. 2019, Inf. Circ., 199, 1
Tokovinin, A. & Briceño, C. 2020, AJ, 159, 15
Tokovinin, A. Cantarutti, R., Tighe, R., et al. 2010b, PASP, 122, 1483
Tokovinin A., Cantarutti, R., Tighe R., et al. 2016b, PASP, 128, 125003
Tokovinin, A., Mason, B. D., & Hartkopf, W. I. 2010a, AJ, 139, 743 (TMH10)
Tokovinin, A., Mason, B. D., & Hartkopf, W. I. 2014, AJ, 147, 123
Tokovinin, A., Mason, B. D., Hartkopf, W. I., et al. 2015, AJ, 150, 50
Tokovinin, A., Mason, B. D., Hartkopf, W. I., et al. 2016a, AJ, 152, 116
Tokovinin, A., Mason, B. D., Hartkopf, W. I., et al. 2018, AJ, 155, 235
Tokovinin, A., Mason, B. D., Mendez, R. A., et al. 2019, AJ, 158, 148
Ziegler, C., Tokovinin, A., Briceño, C., et al. 2020, AJ, 159, 19